Journal of Alloys and Compounds 516 (2012) 41–48

Contents lists available at SciVerse ScienceDirect

Journal of Alloys and Compounds

journal homepage: www.elsevier.com/locate/jallcom

Aqueous starch as a stabilizer in zinc oxide nanoparticle synthesis via laser ablation

Reza Zamiri[a], Azmi Zakaria[a,1], Hossein Abbastabar Ahangar[b], Majid Darroudi[c,2], Ali Khorsand Zak[d], Gregor P.C. Drummen[e,*,1]

[a] Department of Physics, Faculty of Science, Universiti Putra Malaysia, 43400 UPM, Serdang, Selangor, Malaysia
[b] Department of Chemistry, Faculty of Science, Universiti Putra Malaysia, 43400 UPM, Serdang, Selangor, Malaysia
[c] Advanced Materials and Nanotechnology Laboratory, Institute of Advanced Technology (ITMA), Universiti Putra Malaysia, 43400 UPM, Serdang, Selangor, Malaysia
[d] Low Dimensional Material Research Center, Department of Physics, University of Malaya, Kuala Lumpur 50603, Malaysia
[e] Bionanoscience and Bio-Imaging Program, Cellular Stress and Ageing Program, Bio&Nano-Solutions, D-40472 Düsseldorf, Germany

ARTICLE INFO

Article history:
Received 4 October 2011
Received in revised form
18 November 2011
Accepted 24 November 2011
Available online 8 December 2011

Keywords:
Laser ablation
Zinc oxide
Semi-conductor
Nanoparticle
Starch
Stabilizer
Photoluminescence
UV–vis spectroscopy
XRD
FTIR
TEM

ABSTRACT

Zinc oxide is a semiconductor with exceptional thermal, luminescent and electrical properties, even compared with other semiconducting nanoparticles. Its potential for advanced applications in lasers and light emitting diodes, as bio-imaging agent, in biosensors and as drug delivery vehicles, in ointments, coatings and pigments has pulled zinc oxide into the focus of various scientific and engineering research fields. Recently we started investigating if nanoparticle synthesis via laser ablation in the presence of natural stabilizers allows control over size and shape and constitutes a useful, uncomplicated alternative over conventional synthesis methods. In the current paper, we determined the ability of natural starch to act as a size controller and stabilizer in the preparation of zinc oxide nanoparticles via ablation of a ZnO plate in a starch solution with a nanosecond Q-Switched Nd:YAG pulsed laser at its original wavelength ($\lambda = 1064$ nm). Our results show that the particle diameter decreases with increasing laser irradiation time to a mean nanoparticle size of approximately 15 nm with a narrow size distribution. Furthermore, the obtained particle size in starch solution is considerably smaller compared with analogous ZnO nanoparticle synthesis in distilled water. The synthesized and capped nanoparticles retained their photoluminescent properties, but showed blue emission rather than the often reported green luminescence. Evaluation of old preparations compared with freshly made samples showed no agglomeration or flocculation, which was reflected in no significant change in the ZnO nanoparticle size and size distribution. Overall, our experimental results demonstrate that starch can indeed be effectively used to both control particle size and stabilize ZnO nanoparticles in solution.

1. Introduction

Over the past decade, nanostructured semiconductor materials – in the mesoscopic size range such materials display unique optical, electronic, thermal, magnetic, and structural properties not available from individual molecules or bulk solids – have been the focus of intense research for applications in biomedical imaging, biological analysis and sensing, novel therapeutics, and photovoltaic and optoelectronic devices to name but a few. While most research concentrates on CdS, CdSe (II–VI) and GaAs, InAs (III–V) semiconductors as major components in quantum dots, zinc oxide nanoparticles (ZnO-NPs) have only recently become the focus of attention; this despite the fact that ZnO by no means is an unknown material and its properties have been studied since the 1930s. Bulk material ZnO is widely used as an additive in the production of a variety of materials and products, including plastics, ceramics, glass, lubricants, adhesives, paints, ointments, foods (as a source of Zn as a micronutrient), as an UV-filter in sunscreens, and other applications.

Zinc oxide's wide bandgap ($\Delta E_g = 3.37$ eV, $\lambda = 368$ nm) is indicatory for semiconducting properties and responsible for its remarkable optical characteristics, which was recently verified by Fan et al. [1]. ZnO is a compound group II–VI semiconductor with a number of exceptional properties, such as electric conductivity, optical transparency, piezo electricity and nonlinear second-harmonic generation [2–5]. However, it is its large exciton

* Corresponding author. Tel.: +49 (0)211 22 97 36 48; fax: +49 (0)322 22 40 75 00.
E-mail address: gpcdrummen@bionano-solutions.de (G.P.C. Drummen).
[1] Equal contribution.
[2] Current address: Department of Modern Sciences and Technologies, School of Medicine, Mashhad University of Medical Sciences, Mashhad, Iran.

0925-8388/$ – see front matter © 2011 Elsevier B.V. All rights reserved.
doi:10.1016/j.jallcom.2011.11.118

binding energy (59 meV [6]), which allows intense near-band-edge excitonic emission at room temperature (thermal energy ~26 meV) and beyond that has rekindled the interest in this material. Because of this property, its potential as an UV-blue emitter for lasers and diodes becomes obvious, but also in solar cells, gas and biosensors, and is a newly emerging field of study with enormous potential [7–12]. Extensive and excellent reviews on ZnO's properties were recently published by Özgür [10,13], Djurisic [9], Schmidt-Mende [11], and their respective co-workers.

Although very high quality materials are required for the aforementioned applications, recent experience with a number of synthesis methods has shown that the produced nanostructures often deviate from stoichiometric composition, which leads to optically active and undesirable defects formation [11]. Zinc oxide nanoparticles can be synthesized in a myriad of ways, including physical vapor deposition [14], an organometallic precursor method [15], via precipitation [16], solvothermal and hydrothermal methods [17,18], and sol–gel methods such as sol–gel combustion [19,20]. However, most of these techniques are expensive and complex to perform, with limited control over particle size and size uniformity. Pulsed laser ablation of solids in solution (LASiS) has been shown to be an effective, flexible and efficient technique for preparing various types of high purity nanoparticles without surface contamination by residual anions and reducing agents [21–28]. Many reports in the literature show that significant effort is put into adapting this technique in such a way that particle size and shape can efficiently and accurately be controlled. Nonetheless, laser ablation production methods suffer from some of the same drawbacks associated with other production methods in solution, although to a lesser extent, i.e. the propensity for nanoparticle agglomeration, lack of long term stabilization in solution, and the need for capping for easy functionalization.

In the current paper, we investigate whether controlled colloidal preparation of ZnO-NPs in starch solution by laser ablation is feasible and to what extent the ablation time contributes to the final size and overall result. We hypothesized that starch, due to its potential for multi-dentate action via its hydroxyl groups, might be able to interact with ZnO surface charges and as such act as a stabilizing template for nanoparticle synthesis. Furthermore, starch is a natural water-dispersible, biodegradable, inexpensive, and commercially available product and may provide a scaffold for further (bio)functionalization. Synthesized ZnO-NPs were characterized by XRD, FT-IR, UV–vis spectroscopy, fluorometry, and TEM in order to evaluate particle size and size distribution, crystal structure and overall composite structure.

2. Experimental

2.1. Preparation of the ZnO ablation plate

The ZnO plate, as a basis for the ablation, was made by mixing 2 g of ZnO powder with 2 drops of polyvinyl alcohol solution (1% in water) and pressed into plate shape under 300 MPa pressure. Subsequently, the ZnO plates were sintered at 1000 °C in a box furnace for 2 h under atmospheric conditions. Fig. 1 shows a SEM micrograph of the surface of the prepared plate, revealing an average grain size of about 10 μm. It is clearly observable that the target reaches a suitable density and that the grains are a result of the sintering process.

2.2. Synthesis of ZnO nanoparticles by laser ablation

Zinc oxide nanoparticles were prepared via laser ablation using a pulsed Q-Switched Nd:YAG laser (Brilliant B; Quantel, Newbury, UK) with 10 Hz repetition rate, 5 ns pulse duration, 1064 nm wavelength and 350 mJ/pulse output energy. The ZnO plate was placed in a cubic glass cell containing 10 ml starch solution (1% wt) and positioned about 4 mm from the cell wall (Fig. 2A). The laser beam was focused by a 25 cm focal length lens at the ZnO plate and the solution was stirred continuously during the ablation process to disperse the produced NPs. The ablation was performed at different irradiation times (5, 10, 15 and 20 min) to study the effect of the ablation time on the properties of the prepared nanoparticles.

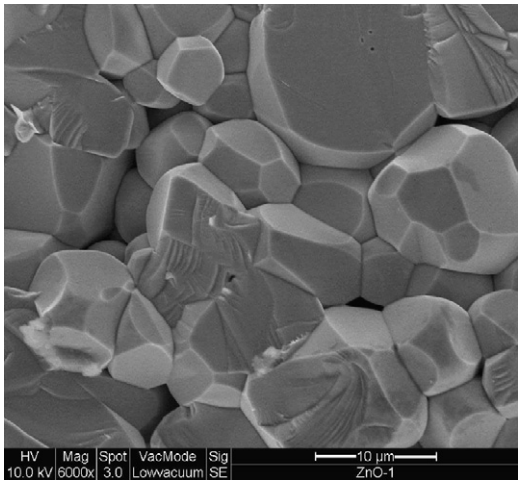

Fig. 1. SEM image showing the surface structure of the prepared ZnO plate.

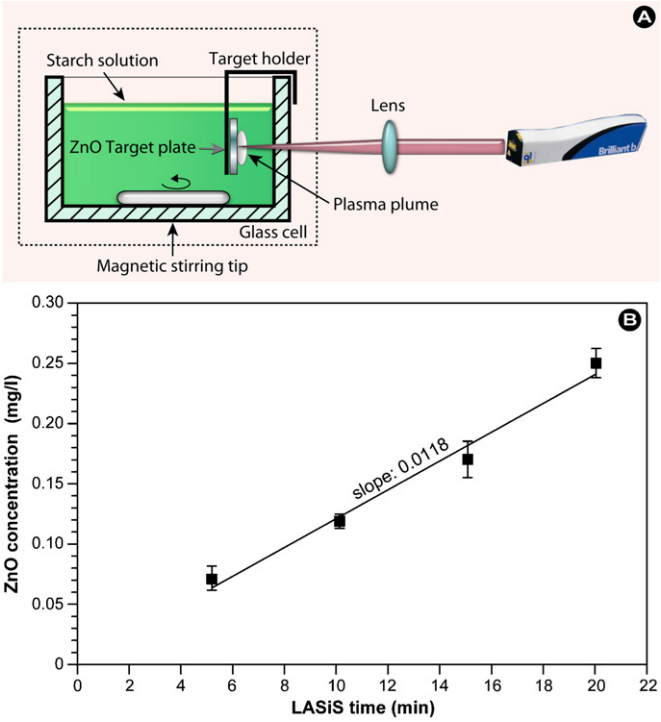

Fig. 2. (A) Schematic representation of the experimental set-up for laser ablation. (B) Determination of the ZnO nanoparticle formation rate.

2.3. ZnO nanoparticle characterization

The prepared ZnO-NPs were initially characterized using an UV–vis double beam spectrophotometer (Shimadzu, Columbia, MD, USA) with 1 cm optical path cell. Approximately 1 ml of the sample was pipetted into a cuvette and spectra were recorded relative to a 1 ml starch (1% wt) solution. An atomic absorption spectrometer (AAS-S Series; Thermo Scientific, San Jose, CA) was used to measure the concentration of Ag-NPs in the starch solution.

FTIR spectra and XRD signals were recorded with a Perkin Elmer 1650 FT-IR spectrometer (Perkin Elmer, Waltham, MA, USA) and a Shimadzu XRD-6000 X-ray diffractometer (Shimadzu, Tokyo, Japan) respectively. For FT-IR and XRD characterization, a powder was made by first centrifuging the colloidal solution, aspirating the fluid, and drying the resulting product in an oven at 100 °C.

Morphological evaluation and measurement of size and size distribution were performed with a Hitachi H-7100 Transmission Electron Microscope (TEM; Hitachi, Chula Vista, CA, USA) operating at an accelerating voltage of 120 kV. The samples were prepared for TEM experiments by depositing a drop of the ZnO-NP colloidal solution onto carbon coated copper grids and left to air dry for one day at ambient temperature.

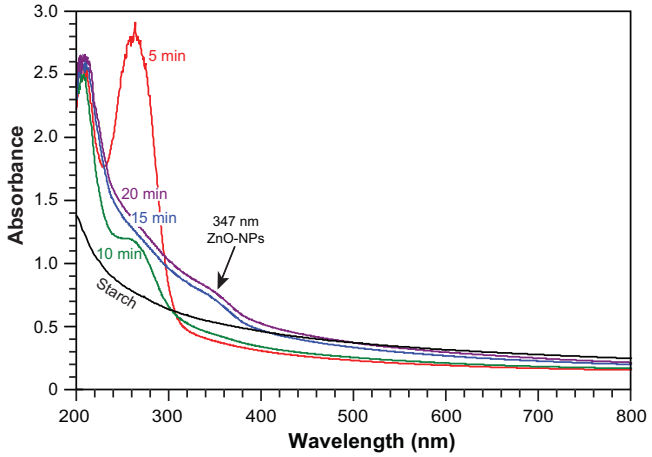

Fig. 3. UV–vis absorption spectra of the starch solution alone and aqueous starch samples containing ZnO-NPs prepared at the indicated ablation times with a pulsed Q-Switched Nd:YAG laser (10 Hz repetition rate, 5 ns pulse duration, 1064 nm wavelength and 350 mJ/pulse output energy).

Zeta potentials of the prepared samples were measured with a Zetasizer 3000HS photon correlation spectrometer (Malvern Instruments Ltd., Malvern, UK) at an applied voltage of 100 V.

Photoluminescence (PL) spectra were recorded with a Perkin-Elmer LS55 fluorescence spectrometer (Perkin-Elmer, Selangor, Malaysia) with a pulsed xenon light source and 320 nm excitation wavelength.

2.4. ZnO nanoparticle separation and collection

The produced ZnO nanoparticles were separated form the aqueous solution by centrifuging the colloidal solution with an Avanti J-25 ultra-centrifuge (Beckman-Coulter Inc., Fullerton, CA, USA) at 75,000 × *g* for 15 min. The resulting powder was further dried and stored in a desiccator at ambient temperature.

2.5. Statistical analysis

The nanoparticle size distribution was analyzed with UTHSCSA ImageTool (Ver. 3). Standard procedures were used to calculate means and standard deviations (SPSS Statistics Software Ver. 17).

3. Results and discussion

Recently, Zeng et al. [29] described that laser ablation of a pure zinc plate in water and aqueous sodium dodecyl sulfate (SDS) led to the formation ZnO–Zn composite nanoparticles. To prevent the formation of a composite rather than the desired ZnO, we opted to prepare a ZnO plate from bulk powder with a high purity through sintering at 1000 °C. This resulted in a ZnO plate with a suitable density (Fig. 1). LASiS of ZnO-NPs from this ZnO-plate occurs through local evaporation of the plate material, leading to the formation of a plasma plume (Fig. 2A), subsequent nucleation during plasma plume cooling for which the driving force is supersaturation, and further crystal growth to the final mean size. By determining the concentration of the ZnO-NPs at various time points via AAS, the formation rate could be calculated from the slope in Fig. 2B. The formation rate was determined to be 11.8 ± 0.8 μg/(l min).

Zinc oxide nanoparticle synthesis via LASiS in starch solution was closely followed by UV–vis spectroscopy. In Fig. 3, the spectra of the starch solution and the produced ZnO-NPs in aqueous starch are depicted. The starch solution alone shows one absorption peak at <200 nm due to $n \rightarrow \sigma^*$ transitions. Approximately 5 min into the ablation of the ZnO plate, a characteristic absorption peak appeared at 264 nm, whose intensity significantly decreased and shifted toward lower wavelengths after 10 min ablation time, only to completely disappear with increasing laser irradiation time. The presence of this peak may be attributed to a layered organic/inorganic nanocomposite containing β-$Zn(OH)_2$ sheets and starch. It is well known from liquid–solid interface studies that interactions at the interface during laser ablation generate high temperature plasma, with high pressure and density [30,31].

Liang et al. [32] earlier described that ejected Zn species undergo aqueous oxidization, which initially leads to the formation of zinc hydroxide and hydrogen radicals ($H^{\bullet}$) and subsequent dehydration to Zn-NPs. Thus the continuous decreasing intensity of the 264 nm peak with increasing ablation time may be due to dehydration of β-$Zn(OH)_2$ to finally form ZnO nanoparticles, which is comparable to solvothermal oxidation of Zn metal [33]. Furthermore, with increasing laser ablation time from 5 to 20 min, the pH of the solution increased from 5.4 to 6.9 according to:

$$ZnO + H_2O \leftrightarrows Zn(OH)_2 \leftrightarrows Zn^{2+} + 2OH^-$$

This pH increase suggests that the produced ZnO nanoparticles are positively charged because the isoelectric point of ZnO is 9.5 in aqueous solution [34]. This notion was further corroborated by zeta potential measurements for the sequential ablation times of 5, 10, 15, and 20, which shows a steady increase from 6.00 to 11.80 mV (6.00, 6.96, 11.80, and 8.17 mV respectively). The decrease in the zeta potential at 20 min ablation time was most likely caused by the steadily increasing pH, which resulted in an increase of negative charge on the nanoparticle's surface. Comparable absorption spectra were also observed in the ablation of Zn plates in an aqueous solution of SDS, which led to β-$Zn(OH)_2$ sheet formation due to strong and direct bonding of charged dodecyl sulfate with Zn-coordinated sites in addition to the preceding aqueous oxidation [35–37]. Such charged and cooperative assemblies involve much stronger interactions, as indicated by the lack of sheet dehydration to ZnO nanoparticles even after 30 min ablation and the pH change from 7.0 to 9.6 [32], compared with the formation of starch-β-$Zn(OH)_2$ complexes in our experiments. The results as presented in Fig. 3 show that as the laser ablation time approaches 15 min, not only does the 264 nm peak recline, but a second weak peak appears at 347 nm, which is characteristic for ZnO-NP growth.

Transmission electron microscopic (TEM) evaluation of the size distribution as a function of the irradiation time (5, 10, 15 and 20 min respectively), as depicted in Fig. 4, shows that overall the particles are spherical, relatively uniform, and that the size decreases significantly with the irradiation time. This irradiation time-dependent size decrease can be explained by the fact that initially formed and suspended ZnO-NPs are fragmented in the laser path by subsequent laser pulses, as reflected by the shift of the Gaussian distribution peak to smaller sizes (Fig. 4). Even though LASiS at 1064 nm in the infra-red is not governed by significant direct absorption of photons by the target, excitation nonetheless occurs due to inverse bremsstrahlung (IB) absorption within the plasma plume, by which the free electrons gain kinetic energy from the laser beam [38,39]. This promotes plasma plume ionization and excitation through collision with excited and/or the ground state neutrals. The IB absorption coefficient in the case of the 1064 nm laser is much higher than for the 532 nm and 355 nm lasers and the excitation temperature is higher for the 1064 nm laser than 532 and 355 nm lasers [40]. After 20 min, mean ZnO-NP sizes smaller than 15 nm with a range from 6 to 28 nm can be observed, with most ZnO-NPs within the population showing sizes below 15 nm (Fig. 4, bottom). In addition, the narrowing of the Gaussian distribution curve reflects a decrease in the size distribution and hence more uniform particles are obtained. The aforementioned reduction in size through fragmentation is corroborated both by Fig. 5, which shows particles of different sizes and a large fragmented particle (grey arrow, insert), and similar experiments and observations with silver nanoparticles [41].

In order to further determine the significance of the starch solution in size distribution and control, reference measurements under

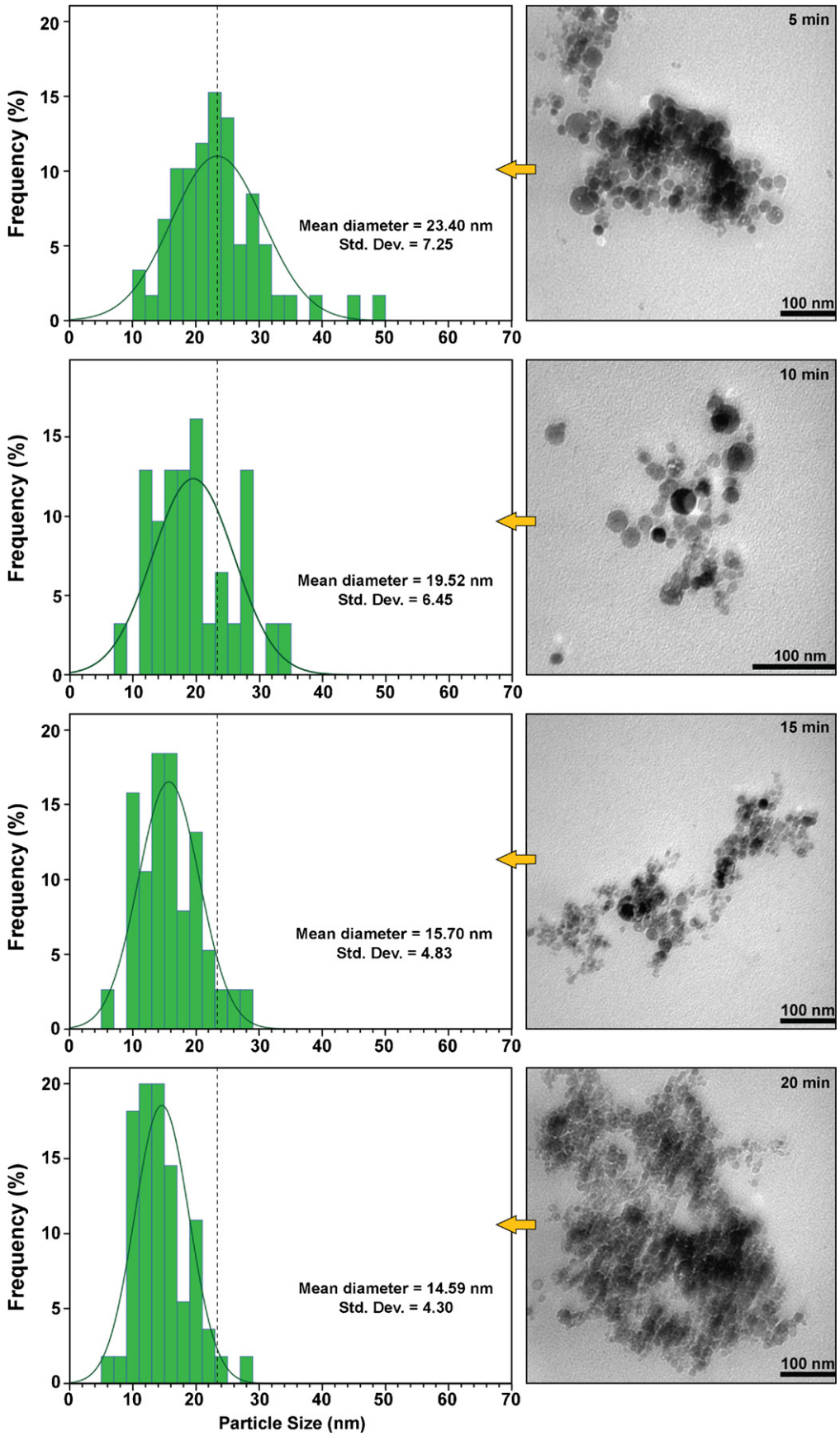

Fig. 4. TEM images and corresponding size distribution of samples prepared at various laser ablation times. Notice the shift in the initial mean size (dotted line) toward smaller values with increasing laser ablation time.

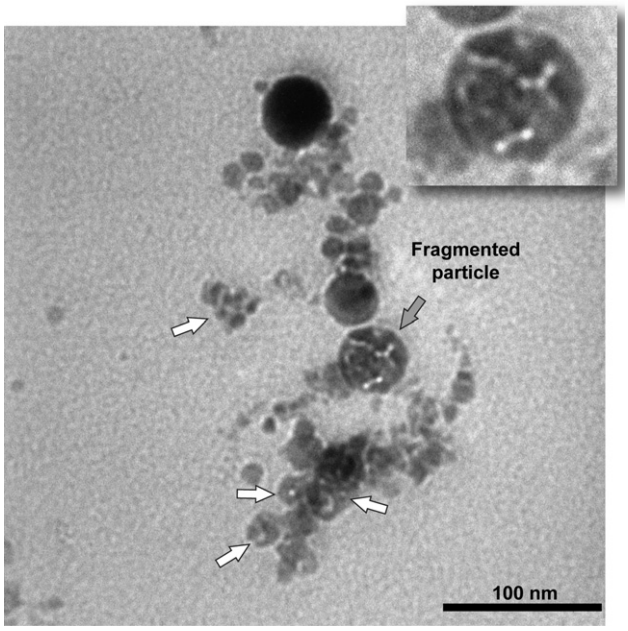

Fig. 5. Electron micrograph showing the process of fragmentation (white arrows) of the NPs by the laser beam irradiation. At the grey arrow and insert, a large cracked particle is seen, which would fragment into several smaller particles upon continued irradiation.

similar experimental conditions were performed with distilled water as a solvent. The TEM images and results of ZnO-NPs size distributions prepared in distilled water are presented in Fig. 6. The obtained particle size was considerably smaller after 20 min LASiS in the starch solution compared with distilled water. In addition, the TEM image in Fig. 6 clearly shows that under these environmental conditions, particle growth leads to deviations from the spherical form, with a more asperous appearance. We attribute the small NP size in starch solution to the interaction between the starch molecules and produced NPs during the laser ablation process. NPs are formed through phase transition, nucleation and crystal growth of the emitted materials [26], such as Zn atoms, ZnO molecules, clusters and droplets from the ZnO plate during the laser ablation process. The starch can adsorb and passivate nanoparticles through electrostatic interaction between its hydroxyl groups with positive surface charges on ZnO [37] and consequently prevents

Table 1
Overview of the lattice parameters of the prepared ZnO-NPs in starch solution and crystal structure of wurtzite.

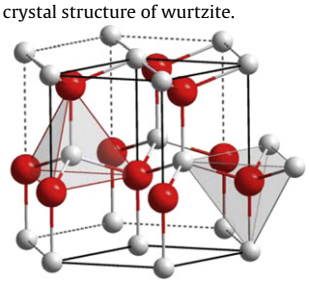

$2\theta \pm 0.01$	$h\,k\,l$	$d_{h\,k\,l}$ (nm) ± 0.0006	Structure
31.66	(1 0 0)	0.2824	Hexagonal
34.22	(0 0 2)	0.2618	
Lattice parameter (nm)		V (nm^3) ± 0.2	Cos φ
$a = 0.3261 \pm 0.0005$ $c = 0.5237 \pm 0.001$ $c/a = 1.606 \pm 0.001$		48.21	0

their aggregation and growth due to steric hindrance by the glucose rings (Fig. 7).

X-ray diffraction analysis (XRD) and Fourier Transform Infrared (FTIR) spectroscopy were used to further characterize the structure of the produced ZnO-NPs and the starch composite. For the analysis and affirmation of the presence of ZnO-NPs, the solution was dried in an oven at 60 °C and the dried powder was subsequently used for XRD analysis. The resulting XRD patterns of prepared samples at 20 min ablation time are shown in Fig. 8. All the detectable peaks can be attributed to a ZnO wurtzite structure (Table 1), which is a common ABAB hexagonal close packed form of nanoscale semiconductors, such as AgI, CdS, CdSe, α-SiC, GaN, and ZnO. The wurtzite structure lacks inversion symmetry (non-centrosymmetric), because of which wurtzite crystals generally display properties such as piezoelectricity and pyroelectricity.

The wurtzite structure consists of a hexagonal unit cell (Table 1) and belongs to the space group C_{6v}^4 (Schoenflies notation) or $P6_3mc$ (Hermann–Mauguin notation) [13]. The wurtzite lattice parameters, e.g., the values of d, the distances between adjacent crystal planes ($h\,k\,l$), were calculated from the Bragg equation:

$$\lambda = 2d\,\sin\theta \quad (1)$$

The lattice constants a, b and c, interplanar angles, the angles φ between the planes ($h_1\,k_1\,l_1$) of spacing d_1 and the plane ($h_2\,k_2\,l_2$)

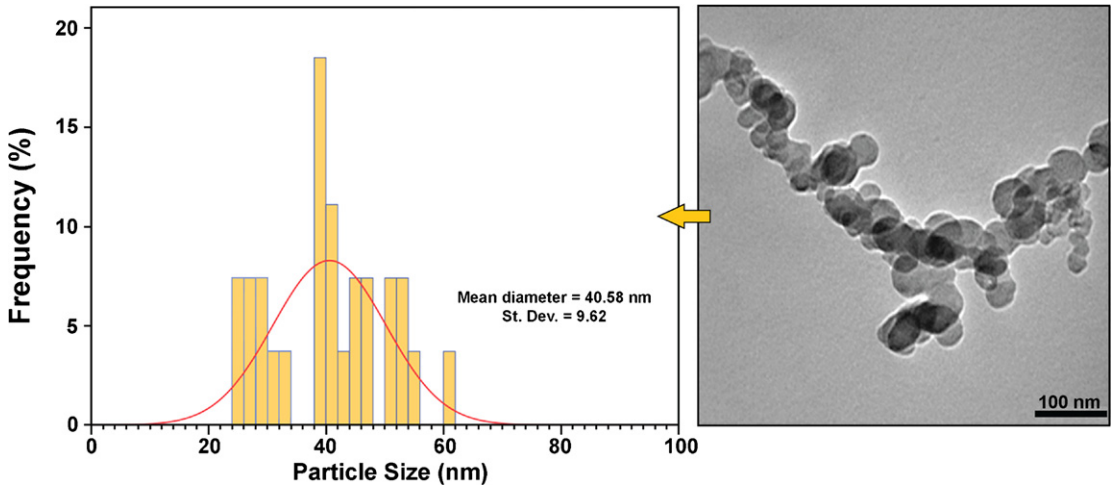

Fig. 6. TEM image and size distribution of reference ZnO-NPs prepared in distilled water (20 min ablation time).

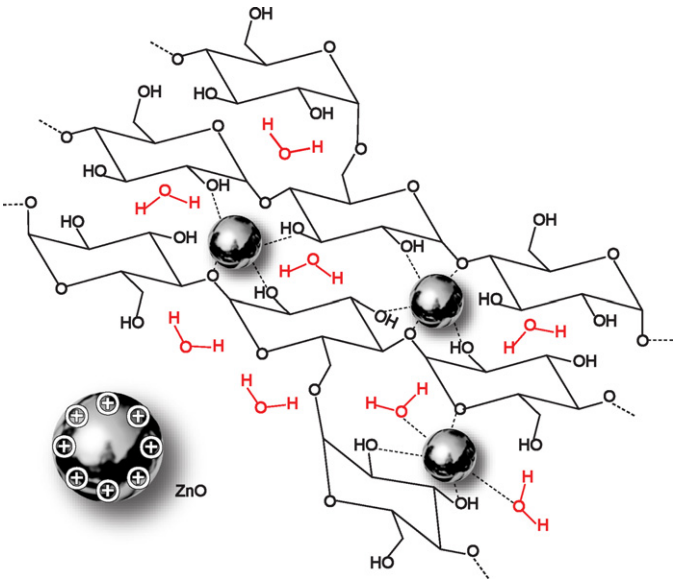

Fig. 7. Schematic representation of the starch–ZnO-NP composite and its stabilizing action.

of spacing d_2 and the primary cell volumes were calculated from the Lattice Geometry equation [42] according to:

$$\frac{1}{d^2} = \frac{4}{3}\left(\frac{h^2+hk+k^2}{a^2}\right) + \frac{l^2}{c^2} \quad (2)$$

$$V = \frac{\sqrt{3}a^2c}{2} = 0.866a^2c \quad (3)$$

$$\cos\varphi = \frac{h_1h_2 + k_1k_2 + \frac{1}{2}(h_1k_2 + h_2k_1) + \frac{3a^2}{4c^2}l_1l_2}{\sqrt{\left(h_1^2 + k_1^2 + h_1k_1 + \frac{3a^2}{4c^2}l_1^2\right)\left(h_2^2 + k_2^2 + h_2k_2 + \frac{3a^2}{4c^2}l_2^2\right)}} \quad (4)$$

The lattice parameters of the ZnO-NPs prepared in starch media are summarized in Table 1. Our results are in agreement with

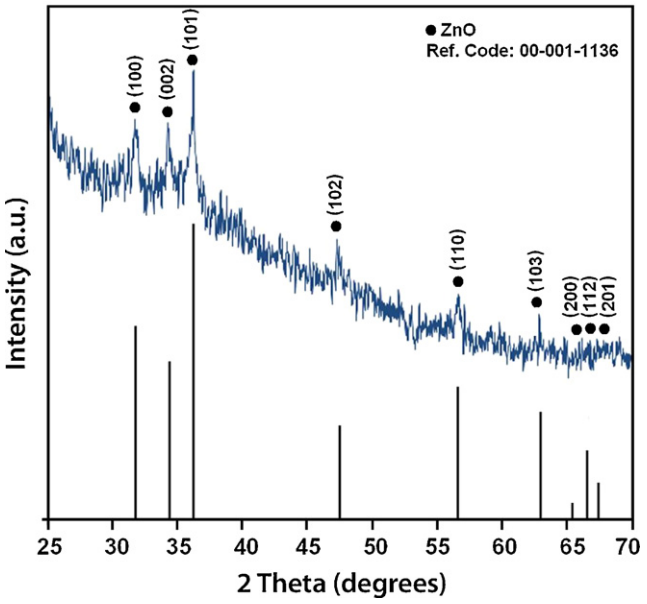

Fig. 8. XRD patterns of samples prepared at 20 min ablation time.

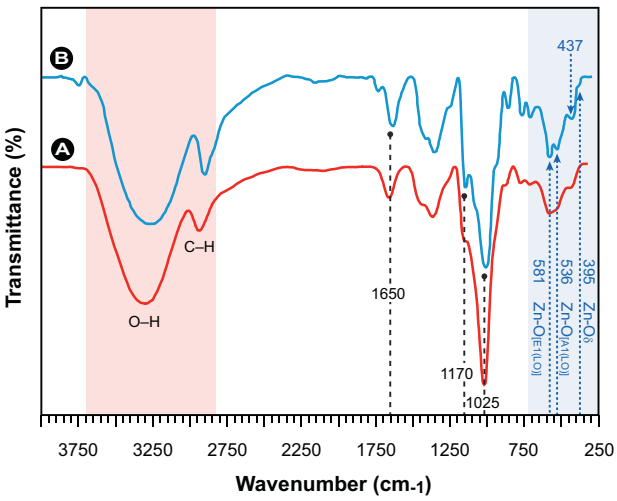

Fig. 9. FTIR spectra of (A) pure starch (B) starch containing ZnO-NPs (dried gel) prepared at 20 min laser irradiation.

lattice parameters previously reported ($a = 0.325$ and $c = 0.52$ nm; ratio $c/a \sim 1.60$) [43]. The ratio c/a of the elementary translation vectors deviates slightly from the ideal value for a hexagonal cell ($c/a_{ideal} = \sqrt{8/3} = 1.633$).

Fig. 9 shows the FTIR spectra of pure starch and starch dried gel containing ZnO-NPs prepared by 20 min laser irradiation. The main starch absorption peaks can be observed between 900 and 1200 cm^{-1}, corresponding to C—O bond stretching in starch. The peaks at 1025 and 1170 cm^{-1} are related to the C—O bond stretching of C—O—C and C—O—H groups in starch respectively [44]. In addition, the two peaks between 2850 and 3700 cm^{-1} may be attributed to C—H and O—H normal vibration modes. An absorption peak identified at 1650 cm^{-1} corresponds to the C=O normal stretching vibration mode. The fact that C=O is demonstrated in the FTIR spectra shows that some of the starch molecules were hydrolyzed to glucose during the process and/or the presence of CO_2. Most importantly, Fig. 9B shows absorption peaks between 400 and 600 cm^{-1}, which are related to Zn—O vibration modes [45]. In bulk wurtzite zinc oxide, the number of atoms per unit cell equals 4 with a total of 12 phonon modes, i.e. 3 longitudinal (LO) and 6 transverse optical (TO), 1 longitudinal (LA) and 2 transverse acoustic (TA). Of these modes, A_1 and E_1 are both Raman and infrared active, which split into LO and TO components with distinct frequencies. In bulk ZnO, the two nonpolar E_2 branches are Raman active only, and the B_1 branches are inactive (silent modes) [13]. The FTIR spectrum in Fig. 9B shows peaks at 536 and 581 cm^{-1} corresponding to [A_1(LO)] and [E_1(LO)] modes respectively. Furthermore, a peak at around 430 cm^{-1}, most often 437 cm^{-1} as in our results, is reported in literature for ZnO nanoparticles as corresponding to the E_2 mode of hexagonal ZnO (Raman active) [45]. The outcome of the FTIR measurements confirms the presence of ZnO-NPs within the starch matrix after laser ablation and is in conformity with the results of the XRD measurements described above.

In order to determine if the formed nanoparticles retained their properties and to further characterize the ZnO-NPs, photoluminescence (PL) emission spectra were recorded as depicted in Fig. 10. Typically, the PL spectrum of ZnO shows near-band-edge UV emission and a broad defect-related visible green emission, although yellow or blue emissions have also been reported [46]. The near-band-edge UV emission of the ZnO-NPs in water at $\lambda_{max} = 357$ nm (3.43 eV) is clearly present, but virtually absent in the starch capped ZnO-NPs and is consistent with the band gap of the ZnO nanoparticles (3.37 eV). The ZnO-NPs–starch spectrum

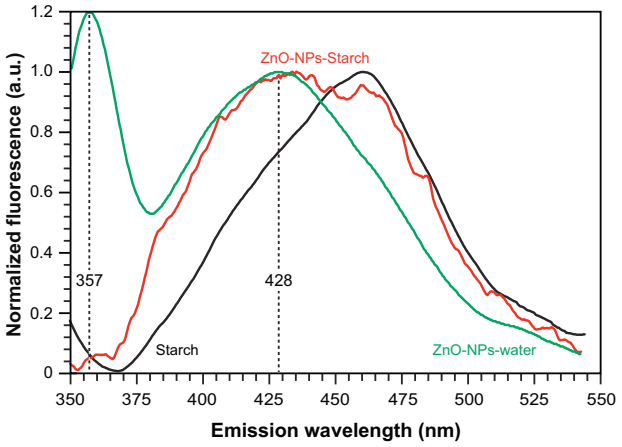

Fig. 10. Fluorescence emission spectra (λ_{ex} = 320 nm) of the starch solution alone, aqueous starch samples containing ZnO-NPs, and ZnO-NPs in water prepared via LASiS for 20 min (pulsed Q-Switched Nd:YAG laser, 10 Hz repetition rate, 5 ns pulse duration, 1064 nm wavelength and 350 mJ/pulse output energy).

shows a broad emission maximum from 420 to 470 nm. From the normalized individual spectra in Fig. 10 it can be seen that both the emission spectrum of ZnO-NPs in water with λ_{max} = 428 nm and the spectrum of starch are part of the ZnO-NPs–starch spectrum.

Zinc oxide's photoluminescence is complex and heterogeneous and affected by the method of synthesis [46], the size of the ZnO-NPs [47], and recently it was reported that ZnO PL contradicts Kasha's rule of excitation wavelength independence of the emission spectrum [48]. Our PL results are generally in agreement with previously reported results for starch-capped ZnO colloids [34] and with an observed blue emission at 428 (ex = 320) nm – indicating a high defect incidence related to deep level emissions, such as Zn interstitials and oxygen vacancies – are comparable with the data reported by Irimpan et al. [48].

Finally, we tested the stability of ZnO-NPs in starch solution by reevaluating samples previously prepared and stored for one month at ambient temperature in the dark. Visual evaluation did not show any significant change in the solution's turbidity or flocculation. TEM images and measurement of the particle size showed negligible variation compared with freshly prepared samples (data not shown). Thus, our experiments substantiate that ZnO-NPs prepared in starch solution remain stabile for prolonged periods of time.

4. Conclusions

Here we report the successful preparation of ZnO-NPs by laser ablation of a ZnO plate in starch solutions under different laser ablation times. The obtained results show that in the presence of starch, significantly smaller ZnO particles can be produced compared with distilled water as a reference environment. The starch acts as a complexing template that both prevents particles formed from aggregating as well as crystal growth through steric hindrance. Furthermore, the starch–ZnO composite ensures a stabile solution over prolonged periods of time. The composite nature however, due to its physicochemical properties, does not exclude further capping steps and functionalization of the formed ZnO-NPs for various purposes, such as targeted drug delivery in vivo, or photoelectric applications. Concomitantly, the particle size can be directly controlled via the ablation time, although in a non-linear fashion. Finally, capping the ZnO-NPs with starch may provide important advantages over other strategies: the capping agent is environmentally friendly and biodegradable; the binding interaction between starch and the NP is governed by weak forces, which may be reversed to release particles from the composite or separate particles; starch would allow place exchange reactions [49] for easy functionalization; lastly, starch-capped NPs can easily be utilized in biomedical applications and pharmaceutical formulations.

In general, we have shown that stabile ZnO-NPs can be produced in an uncomplicated and size-controllable way using laser ablation with starch as a multifunctional stabilizer.

Acknowledgements

The authors thank Dr. Uwe Schmidt for critically reading this manuscript. This work was supported by the Ministry of Higher Education of Malaysia under Research University Grant Scheme No. 05-01-09-0754RU (R.Z.) and an external Collaborative Research Grant NSR-8978 (G.P.D.).

References

[1] W.J. Fan, J.B. Xia, P.A. Agus, S.T. Tan, S.F. Yu, X.W. Sun, J. Appl. Phys. 99 (2006) 013702.
[2] J.H. Choy, E.S. Jang, J.H. Won, J.H. Chung, D.J. Jang, Y.W. Kim, Adv. Mater. 15 (2003) 1911–1914.
[3] M.H. Huang, S. Mao, H. Feick, H. Yan, Y. Wu, H. Kind, E. Weber, R. Russo, P. Yang, Science 292 (2001) 1897–1899.
[4] J.C. Johnson, H.Q. Yan, R.D. Schaller, P.B. Petersen, P.D. Yang, R.J. Saykally, Nano Lett. 2 (2002) 279–283.
[5] H. Ohta, H. Hosono, Mater. Today 7 (2004) 42–51.
[6] D.G. Thomas, J. Phys. Chem. Solids 15 (1960) 86–96.
[7] E.V. Chelnokov, N. Bityurin, I. Ozerov, W. Marine, Appl. Phys. Lett. 89 (2006) 171119–171121.
[8] T. Dittrich, D. Kieven, M. Rusu, A. Belaidi, J. Tornow, K. Schwarzburg, M. Lux-Steiner, Appl. Phys. Lett. 93 (2008).
[9] A.B. Djurisic, A.M.C. Ng, X.Y. Chen, Prog. Quantum Electron. 34 (2010) 191–259.
[10] Ü. Özgür, Y.I. Alivov, C. Liu, A. Teke, M.A. Reshchikov, S. Dogan, V. Avrutin, S.J. Cho, H. Morkoc, J. Appl. Phys. 98 (2005) 041301.
[11] L. Schmidt-Mende, J.L. MacManus-Driscoll, Mater. Today 10 (2007) 40–48.
[12] J.Y. Son, S.J. Lim, J.H. Cho, W.K. Seong, H. Kim, Appl. Phys. Lett. 93 (2008).
[13] M. Hadis, Ü. Özgür, Zinc Oxide: Fundamentals, Materials and Device Technology, first ed., Wiley-VCH, Berlin, 2009.
[14] R. Yousefi, M.R. Muhamad, J. Solid State Chem. 183 (2010) 1733–1739.
[15] W. Chen, Y.H. Lu, M. Wang, L. Kroner, H. Paul, H.J. Fecht, J. Bednarcik, K. Stahl, Z.L. Zhang, U. Wiedwald, U. Kaiser, P. Ziemann, T. Kikegawa, C.D. Wu, J.Z. Jiang, J. Phys. Chem. C 113 (2009) 1320–1324.
[16] Q. Yang, W. Hu, Ceram. Int. 36 (2010) 989–993.
[17] P. Tonto, O. Mekasuwandumrong, S. Phatanasri, V. Pavarajarn, P. Praserthdam, Ceram. Int. 34 (2008) 57–62.
[18] J. Wang, N. Shi, Y. Qi, M. Liu, J. Sol-Gel Sci. Technol. 53 (2010) 101–106.
[19] S.S. Alias, A.B. Ismail, A.A. Mohamad, J. Alloys Compd. 499 (2010) 231–237.
[20] A.K. Zak, M.E. Abrishami, W.H. Abd Majid, R. Yousefi, S.M. Hosseini, Ceram. Int. 37 (2011) 393–398.
[21] M. Darroudi, M.B. Ahmad, R. Zamiri, A.H. Abdullah, N.A. Ibrahim, K. Shameli, M. Shahril Husin, J. Alloys Compd. 509 (2011) 1301–1304.
[22] P.V. Kazakevich, A.V. Simakin, V.V. Voronov, G.A. Shafeev, Appl. Surf. Sci. 252 (2006) 4373–4380.
[23] J. Neddersen, G. Chumanov, T.M. Cotton, Appl. Spectrosc. 47 (1993) 1959–1964.
[24] M. Sakamoto, M. Fujistuka, T. Majima, J. Photochem. Photobiol. C: Photochem. Rev. 10 (2009) 33–56.
[25] T. Sasaki, Y. Shimizu, N. Koshizaki, J. Photochem. Photobiol. A: Chem. 182 (2006) 335–341.
[26] G.W. Yang, Prog. Mater. Sci. 52 (2007) 648–698.
[27] R. Zamiri, B.Z. Azmi, A.R. Sadrolhosseini, H.A. Ahangar, A.W. Zaidan, M.A. Mahdi, Int. J. Nanomed. 6 (2011) 71–75.
[28] R. Zamiri, A. Zakaria, H.A. Ahangar, A.R. Sadrolhosseini, M.A. Mahdi, Int. J. Mol. Sci. 11 (2010) 4764–4770.
[29] H.B. Zeng, W.P. Cai, Y. Li, J.L. Hu, P.S. Liu, J. Phys. Chem. B 109 (2005) 18260–18266.
[30] T. Sakka, S. Iwanaga, Y.H. Ogata, A. Matsunawa, T. Takemoto, J. Chem. Phys. 112 (2000) 8645–8653.
[31] S. Zhu, Y.F. Lu, M.H. Hong, Appl. Phys. Lett. 79 (2001) 1396–1398.
[32] C.H. Liang, Y. Shimizu, M. Masuda, T. Sasaki, N. Koshizaki, Chem. Mater. 16 (2004) 963–965.
[33] Y.D. Li, X.F. Duan, Y.T. Qian, L. Yang, M.R. Ji, C.W. Li, J. Am. Chem. Soc. 119 (1997) 7869–7870.
[34] N. Vigneshwaran, S. Kumar, A.A. Kathe, P.V. Varadarajan, V. Prasad, Nanotechnology 17 (2006) 5087–5095.
[35] A. Henglein, M. Gutierrez, E. Janata, B.G. Ershov, J. Phys. Chem. 96 (1992) 4598–4602.
[36] S.C. Singh, R. Gopal, Bull. Mater. Sci. 30 (2007) 291–293.

[37] H. Usui, Y. Shimizu, T. Sasaki, N. Koshizaki, J. Phys. Chem. B 109 (2005) 120–124.
[38] S. Amoruso, et al., J. Phys. B: At. Mol. Opt. Phys. 32 (1999) R131.
[39] A. Bogaerts, Z. Chen, Spectrochim. Acta B 60 (2005) 1280–1307.
[40] N.M. Shaikh, S. Hafeez, M.A. Baig, Spectrochim. Acta B: At. Spectrosc. 62 (2007) 1311–1320.
[41] M. Darroudi, M.B. Ahmad, R. Zamiri, A.H. Abdullah, N.A. Ibrahim, A.R. Sadrolhosseini, Solid State Sciences 13 (3) (2011) 520–524.
[42] A.K. Zak, W.H. Abd Majid, M. Darroudi, R. Yousefi, Mater. Lett. 65 (2011) 70–73.
[43] U. Rössler, Landolt-Börnstein, New Series, Group III, Springer, Heidelberg, 1999.
[44] R. Kizil, J. Irudayaraj, K. Seetharaman, J. Agric. Food Chem. 50 (2002) 3912–3918.
[45] G. Xiong, U. Pal, J.G. Serrano, K.B. Ucer, R.T. Williams, Phys. Status Solidi C 3 (2006) 3577–3581.
[46] Y. Gong, T. Andelman, G. Neumark, S. O'Brien, I. Kuskovsky, Nanoscale Res. Lett. 2 (2007) 297–302.
[47] L. Irimpan, V.P.N. Nampoori, P. Radhakrishnan, A. Deepthy, B. Krishnan, J. Appl. Phys. 102 (2007).
[48] L. Irimpan, B. Krishnan, A. Deepthy, V.P.N. Nampoori, P. Radhakrishnan, J. Phys. D: Appl. Phys. 40 (2007) 5670–5674.
[49] A.C. Templeton, S.W. Chen, S.M. Gross, R.W. Murray, Langmuir 15 (1999) 66–76.